$[Cu_6(NGuaS)_6]^{2+}$ and its Oxidized and Reduced Derivatives: Confining Electrons on a Torus

Matthias Witte,[a] Martin Rohrmüller,[b] Uwe Gerstmann,[b] Gerald Henkel,[c] Wolf Gero Schmidt,[b] and Sonja Herres-Pawlis *[a]

The hexanuclear thioguanidine mixed-valent copper complex cation $[Cu_6(NGuaS)_6]^{+2}$ (NGuaS = o-$SC_6H_4NC(NMe_2)_2$) and its oxidized/reduced states are theoretically analyzed by means of density functional theory (DFT) (TPSSh + D3BJ/def2-TZV (p)). A detailed bonding analysis using overlap populations is performed. We find that a delocalized Cu-based ring orbital serves as an acceptor for donated S *p* electrons. The formed fully delocalized orbitals give rise to a confined electron cloud within the Cu_6S_6 cage which becomes larger on reduction. The resulting strong electrostatic repulsion might prevent the fully reduced state. Experimental UV/Vis spectra are explained using time-dependent density functional theory (TD-DFT) and analyzed with a natural transition orbital analysis. The spectra are dominated by MLCTs within the Cu_6S_6 core over a wide range but LMCTs are also found. The experimental redshift of the reduced low energy absorption band can be explained by the clustering of the frontier orbitals. © 2017 Wiley Periodicals, Inc.

DOI: 10.1002/jcc.24798

Introduction

The dinuclear M_2X_2 metal ring structure of the form $[M_2(\mu\text{-}XR_n)_2L_n]$ is a common motif in bioinorganic chemistry and the coordination of the metal is directly related to its functionality.[1–4] Copper often uses this form playing an important role as redox center and is, next to iron, with no doubt one of the most important and fascinating ones and its variety of mechanisms have been widely studied and understood.[5] Especially thiolate coordinated Cu compounds are important electron transfer centers.[6,7] These compounds have been elaborately studied and a high covalency of this interaction has been found.[8–13] A popular representative is the Cu_A complex as found in cytochrome c oxidase or the nitrous oxide reductase.[14–21] The diamond shaped Cu_2 core is bridged by two cysteinate ligands. Electron paramagnetic resonance (EPR) showed that the core is in a mixed valent $Cu^{1.5+}\ldots Cu^{1.5+}$ state, featuring a characteristic seven line pattern. This indicates the single electron to be delocalized over the diamond core.[22,23] A redox active model complex has been synthesized by Duboc and coworkers.[24]

A further class of important complexes in biology are the cysteine-rich metallothioneins incorporating several metal atoms.[25–27] Especially the structure of copper thionein (Cu-MT) has been unraveled by Mangani, Weser et al. and it is found to have six trigonally and two diagonally coordinated Cu(I) ions bound to ten cysteine ligands.[28] It is proposed that Cu-MT acts as copper binder, if the copper concentration in the environment is too high and releases copper under scarce conditions. This is in accordance with the general view that metallothioneins are detoxifying.[29,30] Marchiò et al. synthesized polynuclear Cu(I) complexes with *N*,*N*′S-donor ligands having striking similarities to the Cu-MT.[31]

Recently Cu(I) complexes have drawn attention due to their optical properties. Based on the luminescence, the non-toxicity and their low costs they are promising candidates for OLEDs, resonators for organic lasers, photocatalysts or chemical sensors.[32] A $[Cu(I)_3(mpymt)_3]_2$ (Hmpymt = 4-methylpyrimidine-2-thione) has been synthesized where the two Cu_3S_3 rings form a cylindrical cone. Its fluorescence signal is sensitive to nitrobenzene, nitrotoluene and Fe^{3+}.[33]

In the bioinorganic context, Henkel and coworkers synthesized the structurally inspired Cu_A model complex $Cu(II)_2(NGuaS)_2Cl_2$ (with NGuaS = o-$SC_6H_4NC(NMe_2)_2$).[34] The complex has been theoretically studied in detail with respect to the broken symmetry (BS) minimum energy wave function, its bonding mechanism and the spectroscopic features.[35,36] It is known that nitrogen bases, guanidine ligands in special, serve as good donors in metal bonding.[37–44] Hence, the ligand has been used to synthesize further polynuclear complexes, especially the complex cation $[Cu_6(NGuaS)_6]^{2+}$ which is redox-active and enables the overall charges $n = 1+/2+/3+$.[45] In this work, we utilize density functional theory (DFT) to study the bonding mechanism within the complex cations and its optical properties. From now on, we will use the short form

[a] *M. Witte, S. Herres-Pawlis*
Lehrstuhl für Bioanorganische Chemie, Fachgruppe Chemie, RWTH Aachen University, Landoltweg 1, Aachen 52074, Germany
E-mail: sonja.herres-pawlis@ac.rwth-aachen.de
[b] *M. Rohrmüller, U. Gerstmann, W. G. Schmidt*
Lehrstuhl für Theoretische Physik, Universität Paderborn, Warburger Str. 100, Paderborn 33098, Germany
[c] *G. Henkel*
Lehrstuhl für Anorganische Chemie, Universität Paderborn, Warburger Str.100, Paderborn 33098, Germany
Contract grant sponsors: Deutsche Forschungsgemeinschaft (FOR1405), Paderborn Center for Parallel Computing (PC2), Leibnitz Rechenzentrum der Bayerischen Akademie der Wissenschaften (LRZ), and Regionales Rechenzentrum der Universität Köln (RRZK)

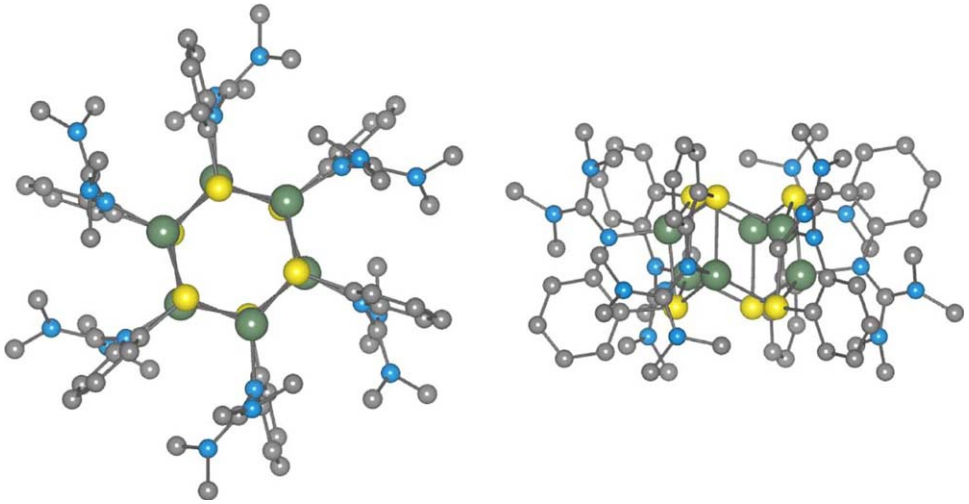

Figure 1. Picture of the $[Cu_6(NGuaS)_6]^{+2}$ complex through *z*-axis (left) and *xy*-axis (right) view, hydrogen atoms are omitted. [Color figure can be viewed at wileyonlinelibrary.com]

$[Cu_6L_6]^n$ (L = NGuaS; n = 0/1+/2+/3+) for the differently charged states.

Methods

Computational methods

The DFT as well as the time-dependent density functional theory (TD-DFT) calculations presented here are accomplished with the Gaussian09 software package, revision D.01.[46] The TPSSh exchange and correlation functional[47–49] has been found to yield a reliable molecular structure as well as optical spectra for related complexes.[35,36] Furthermore, it has been shown that it reproduces accurate densities which is important as we perform detailed bonding and transition analyses.[50] The inclusion of dispersion interaction is particularly vital for the determination of the correct structure in gas phase.[35] The dispersion forces are modeled here using the post-scf method by Grimme with the Becke and Johnson damping.[51,52] The basis set is described with a split valence triple zeta basis with added polarization functions within the formulation of Weigend and Ahlrichs (def2-TZVp) on the Cu, S, and N atoms.[53,54] On the C and H atoms the polarization functions have been dropped to keep the calculations manageable for this large system. The presented results were solely obtained within these approximations if not stated otherwise.

The optical absorption is calculated with the Casida equation originating from the linear response theory in the TD-DFT framework.[55,56] The solvent is modeled implicitly by a polarizable continuum model (PCM)[57–59] and the transition analysis has been done in the framework of natural transition orbitals (NTOs).[60]

For further analysis, Wiberg bond indices (AO basis) as well as the charge decomposition analysis (CDA) are performed with the AOMix program package.[61,62] For the CDA, we split the molecule into two fragments and analyze how the molecular orbitals (MOs) are composed of the fragmental orbitals (FOs). To interpret the bonding character, the overlap *S* and the (total) overlap population (T)OP are calculated, as done for the dinuclear species.[36]

Results and Discussion

The present study is divided into two sections. The first part is devoted to the geometric and electronic structure and the corresponding chemical bonding within the complex in its different oxidations states. The second half discusses the spectroscopic features and compares the UV/Vis absorption spectra for the differently charged states.

Minimum energy wave function

The complex cation is shown in Figures 1 and 2. Formally one would assign two of the Cu ions an oxidation state of +II and the remaining four +I. This might lead to the assumption that an antisymmetric spin coupling emerges which has to be treated by an open shell BS wave function as proposed by Noodleman[63–66] as it is already found in the related Cu_2S_2 diamond core.[35] The study of the dinuclear copper core shows that the minimum wave function is described by a BS wave function. Conversely, it has been shown that a BS state only occurs for larger Cu...Cu/S...S distance pairs than observed for the hexanuclear core. Nevertheless, this has been verified by a BS fragmented guess wave function where the upper as well as the lower Cu_3S_3 part of the ring have a non-vanishing spin density oppositely directed along the *z*-direction (see Fig. 2). However, the wave function converges into the closed-shell case. This does not necessarily mean that there do not exist more complex non-collinear solutions where, for example, the spins are circularly aligned around the Cu_3 S_3 rings but this is beyond the scope of this article. Nevertheless, we have made a wave function stability analysis according to Bauernschmitt and found no instabilities reassuring the ground state nature of the wave function.[67,68] The species with an uneven electron number (3+ and 1+) are treated as $S = 1/2$ open shell systems resulting in states with

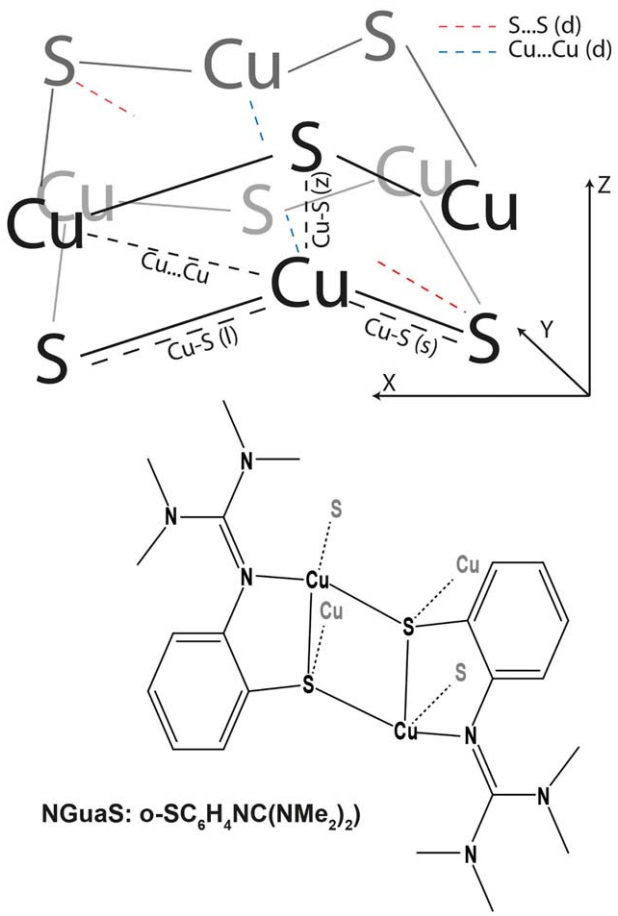

Figure 2. Top: Schematic drawing of the cylindrical Cu_6S_6 hexanuclear core of the complex. Important structure parameters are labeled. Bottom: Projected Lewis structure of a fragment of the complex visualizing the NGuaS ligand. [Color figure can be viewed at wileyonlinelibrary.com]

an $<S^2> = 0.75$ expectation value. This means that there is a single unpaired electron, in accordance with the measured EPR activity, which is discussed later.[45]

Geometry of the different charged states

The complex is, as described in Refs. 45, 69 composed of two Cu_3S_3 rings which are on top of each other and shifted by one atom so that a S atom is on top of a Cu atom. These two rings form a cylindrical hexagon (compare Fig. 2) where the two stacked Cu and S atoms along the *z* direction are connected by a NGua ligand. The correct ground state structure has been verified by normal mode analysis where no imaginary frequencies have been observed. The relaxed cartesian coordinates are given in Supporting Information Table S1.

Each copper or sulfur atom is bound to four partners. Important interatomic distances characterizing the complex are summarized in Table 1 and the different bonds are shown in Figure 2. At first glance, the direct bonding lengths are in very good agreement. For each of the three Cu—S and S—C bonds the absolute value of deviation is less than 0.007 Å. For the direct Cu—N bonds the deviation is −0.02 Å. Only for the direct Cu. . .Cu distance we encounter a deviation of 0.06 Å. As the TPPS(h) functional is the meta-hybrid functional with the least empirical parameters and most fulfilled analytical limits,* we stick to this functional and analyze how far the fraction of exact exchange E^x influences the bond lengths. The results for the $[Cu_6L_6]^{+2}$ case are compiled in Table 2. It appears that the fraction of exact exchange E^x only plays a minor role for the geometric structure and mainly influences the metal-metal interaction that is spatially at a rather long scale. Going from the pure meta GGA TPSS with 0% exact E^x to the TPSSh functional (10% E^x) up to a modified version with 20% exact E^x the Cu—S (l/s) bond lengths are shortened only by 0.01 Å. The Cu. . .Cu distance on the other side elongates by about 0.06 Å for every ten percent of exact exchange. Of course, one could test any combination of different functionals and basis sets until one finds a better suiting pair, but as every bond is overestimated, we are facing a systematical issue and the general description is trustworthy. The difference in the geometry is most likely related to stacking effects, which occur in the solid state phase. In contrast, the classical GGA functional PBE has been tested: all bonds are more or less overestimated.

The complex is found to have a C_i point group to which the Hamiltonian is restricted from now on. This indicates that on each Cu_3S_3 ring one Cu(II) is located among two Cu(I) ions. Dropping the accuracy to 0.02 Å the classification of a S_6 point group becomes available. This means that the difference in oxidation states, hence charge, is an overlying perturbation to a wave function where every copper ion is contributing equally. This is also reflected in the bond length: For the 2+ species two of six Cu—S bond lengths are 0.001 Å smaller than the other four. The difference vanishes for the double reduced state. This is a first hint for delocalization of the electrons over the ring. For a more detailed analysis, we have to take a closer look at the orbitals and charges. We find that the Cu—S bonds in the *xy*-plane are elongated when the complex is further reduced, whereas the Cu. . .Cu-*xy* distances are shortened. This means that the Cu atoms are drawn together whereas the S atoms are pushed slightly outwards, as shown in Figure 3 along with the *xy*-projected distances of the S atoms. This can be explained by putting more electrons in the anti-bonding LUMO (see S2 for all HOMOs and LUMOs). The S—C bond does not change upon oxidation or reduction, which means that no change is induced in the electronic structure there. The Cu—N bond on the other side is becoming longer on reduction. The interpretation is that the donor function of the N_{gua} atom is reduced as more electrons are in the Cu_6S_6 ring and donation becomes less favorable due to electronic repulsion. To verify our intuition of delocalized electrons within the Cu_6S_6 torus, we integrate the charge density within this region on a fine grid with a lateral spacing of $\Delta r = 0.1\ a_0$. The confinement is given by a cylindrical cage, where the height as well as the radius is given by the top S atom. In *z*-direction we add and in *r*-direction we subtract the covalent radius. For all oxidation states, this ensures that we do not count any core or localized S or Cu electrons, see Figure 3. We indeed find that there is a

*In the meantime the improved SCAN functional has been published fulfilling more analytical limits as well as appropriate norms.[70]

Table 1. Averaged geometric parameters of the experimental structure and the different calculated charged states (TPSSh + D3BJ/def2-TVZp).

Complex charge	Cu-S (l)	Cu-S (s)	Cu-S (*z*)	Cu...Cu	Cu...Cu/S...S (d)	Cu-N	S-C
$[Cu_6L_6]^{2+}$ (Exp.) [45]	2.3036(8)	2.2864(9)	2.4346(7)	2.5978(4)	4.5678(5)/5.1857(1)	2.002(3)	1.774(3)
$[Cu_6L_6]^{3+}$	2.314	2.295	2.411	2.568	4.543/5.193	1.984	1.771
$[Cu_6L_6]^{2+}$	2.307	2.292	2.428	2.533	4.467/5.240	2.018	1.771
$[Cu_6L_6]^{1+}$	2.332	3.306	2.435	2.529	4.458/5.317	2.037	1.774
$[Cu_6L_6]^{0}$	2.384	2.319	2.434	2.529	4.470/5.409	2.054	1.771

All values are given in Å, whereas L = NGuaS.

not negligible amount of charge stored. It ranges from 1.5 e^- for the double reduced $[Cu_6L_6]^0$ state down to 1.0 e^- for the oxidized $[Cu_6L_6]^{3+}$ state. Further insight is gained by looking at 2D density slices through a plane given by the three Cu ions in either the top or bottom Cu_3S_3 ring, see Figure 4. Within the inner core there is no increase in the charge density visible, hence the increased accumulated charge originates from the enlarged integration area, being directly related to the increased bond lengths between the Cu and S ions. Furthermore, it is visible that the Cu ions form a fully delocalized ring where the charge can freely spread. Going to lower oxidation states, the charge distribution becomes less in between the Cu ions indicating already a bond breaking. Considering that the double reduced state is experimentally not observable one could speculate that the Cu_6S_6 cage becomes on the second reduction electrostatically unstable in its confined form due to the electrostatic repulsion pushing the cage outwards, destabilizing the delocalized bond of the confined electrons on the Cu ring.

Orbital and bonding analysis

To understand the characteristic geometry of the complex we have to look at the MOs of the complex. The bonding mechanisms are quite complex and at first glance one notices that the occupied frontier orbitals show no distinctive bonding character, but are of rather Cu—S antibonding character as found for the diamond core. For a detailed analysis of the involved mechanisms, we pursue the methodology used for the diamond core species.[36] A first look at the Wiberg bond orders (WBOs) and total overlap populations (TOP), Table 3, shows that within one Cu_3S_3 ring both Cu—S sites are of bonding nature. The Cu—S bond in *z*-direction is bonding, although it is the longest Cu—S bond in the complex and very weak according to TOP and WBO. This already indicates that this bond is mainly binding the two Cu_3S_3 rings. In contrast, the total Cu...Cu interaction is nonbonding as indicated by the non-vanishing negative TOP. Compared to Cu(I)-thiolate heteroadamantane structures one finds similar values. For comparable Cu...Cu distances, Oppermann et al. calculated WBOs of around 0.11.[71]

Furthermore, the Cu—N bond order is around 0.26 for a bond length of 2.1 Å. The Cu—S bonds conversely seem just a little bit weaker with a bond order of 0.4 for trigonal planar coordination and 0.5 for linear coordinated Cu.[71] To understand these differences, we performed a detailed CDA analysis. Contrary to the di-copper core, where only one fragmentation is performed analyzing how the Cu ions interact with the NGuaS donors,[36] we additionally performed a second CDA fragmentation. In this case the molecule is split into two $Cu_3(NGuaS)_3$ fragments. This has the advantage that not only Cu...S interactions can be identified but also three body interactions like bonding Cu–S-Cu delocalized MOs. Throughout the evaluation, only MOs with a TOP greater than 0.10 e^- are considered. The fully illustrated FO decomposition can be found in Supporting Information Figures S3 and S4.

We start with the classical metal-ligand, Cu-NGuaS, interaction. One finds two different bonding mechanisms, covalent and donor–acceptor bonding. The latter one is characterized by MOs which are composed of occupied NGuaS FOs and unoccupied Cu FOs and contributes a TOP of 0.24 e^- to the bonding between the metal and the whole ligand. The covalent TOP is around 0.79 e^-. Hence, the covalent bonding mechanism is thrice as

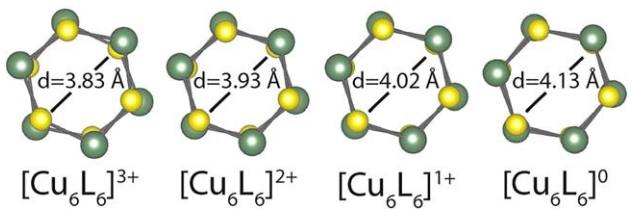

Figure 3. Visualization of the cage atoms for the differently charged states and the *xy*-projected distance of opposing S atoms, with L = NGuaS. [Color figure can be viewed at wileyonlinelibrary.com]

Table 2. Averaged geometric parameters for the PBE and TPSS(h) functional with different fractions of exact exchange E^x for the $[Cu_6L_6]^{2+}$ species, given in Å with L = NGuaS.

Functional, in parenthesis percentage of E^x	Cu-S (l)	Cu-S (s)	Cu-S (*z*)	Cu...Cu	Cu...Cu/S...S (d)	Cu-N	S-C
Exp. [45]	2.3036(8)	2.2864(9)	2.4346(7)	2.5978(4)	4.5678(5)/5.1857(1)	2.002(3)	1.774(3)
PBE (0)	2.315	2.303	2.442	2.573	4.524/5.263	2.027	1.778
TPSS (0)	2.306	2.292	2.431	2.527	4.452/5.247	2.017	1.778
TPSSh (10)	2.307	2.292	2.428	2.533	4.467/5.240	2.018	1.771
TPSSh (20)	2.307	2.291	2.425	2.538	4.477/5.235	2.018	1.764

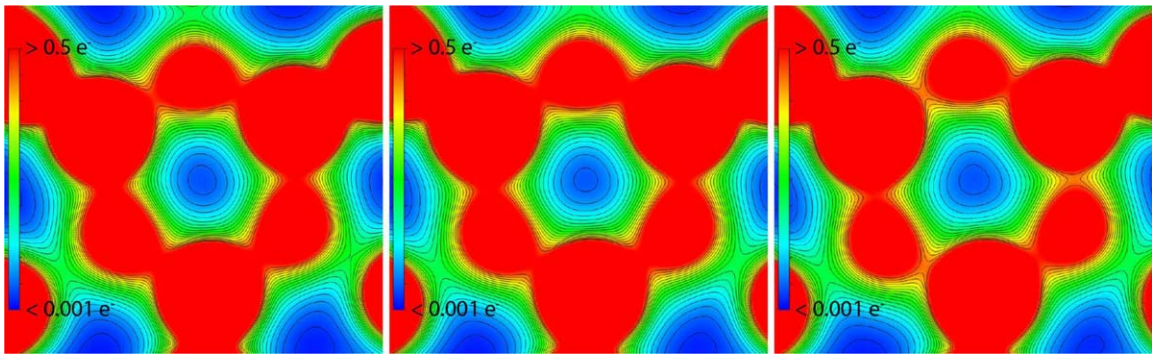

Figure 4. Density slices through an *xy*-Cu_3-plane of the $[CuL]^{3+}$ (left), $[CuL]^{2+}$ (middle), and $[CuL]^{0}$ (right) species. Contour interval is given by 0.0025 e^-. [Color figure can be viewed at wileyonlinelibrary.com]

stabilizing as the donor–acceptor interaction. It is important to mention that the polarization functions on —at least —the Cu and S atoms are important! If they are neglected the bonding mechanism of the core becomes much more coordinative at a ratio one to one compared to covalent bonding. This is reflected in smaller WBOs/TOPs and longer bond lengths respectively, see Supporting Information Table S5.

Here, the L + 1 up to the L + 14 are accepting FOs whereas the L + 1, L + 4, and L + 5 contribute with more than half the DA-TOP in the complete bonding defragmentation scheme (Supporting Information Figure S3), hence are more important. The donor FOs conversely are widely spread over 12 different FOs and range from the H-9 to the H-233. The H-11 and H-41 reappear thrice. An illustration of them is given in Figure 5. Immediately one can see that the important acceptor FOs are Cu *4s* orbitals, especially the L + 1 plays an important role as it contributes a fully delocalized FO forming delocalized MOs over the core region which stabilize the core in total. The other two FOs form Cu S σ bonds along the Cu S short and long bonding axis along with bonds in the Cu S *z* direction (see MO H-69 and H-70). The covalent part of the bonding interaction is, once more, distributed over a variety of more than ten FOs for each fragment. Only the Cu_6 FOs H-17, H-18, H-19, and H-22 occur predominantly and are shown with the H-4, H-5, H-6, and H-11 FOs of the $(NGuaS)_6$ fragment in Figure 6. As expected, the covalent interaction is distributed via Cu *d* and S *p* MOs. The Cu_6 fragment contributes one Cu-Cu bonding FO, H-17, over the whole Cu_6 ring. Two further FOs where three copper are bound by *d*-lobes, see FOs H-18 and H-19, Figure 6. The H-22 is a strongly antibonding FO, having d_z^2-orbitals aligned along the *z*-axis, see Figure 6. They tend to form Cu-S σ-bonds along the *z*-direction, see MO H-61 and H-64. All bonding interactions for this fragmentation are given in Supporting Information Figure S3.

The second fragmentation describes bonding interactions between the Cu and S or N atoms, respectively. The latter one is formally already included in the other fragmentation. Nevertheless we find several new bonding MOs: H-34 H-43 to H-46 and a lower lying block H-82, H-93, and H-94, see Supporting Information Figure S4 for a full list of all new bonding MOs where the FO interactions are shown. The first block shows interesting interactions incorporating the Cu_6S_6 core. Although the overall Cu. . .Cu interaction is antibonding, these MOs are responsible for neighboring Cu ions being bound to each other and form delocalized bonding MOs over the whole Cu_6 torus. The most dominant Cu. . .Cu binding FOs are made up by Cu-$d_{\phi z}$ and d_z^2 FOs.[†] If the complex is reduced these bonding MOs become weaker as can be seen by the more negative TOP. This holds also for the Cu—S (*z*) bond, which elongates on oxidation, hence becomes weaker. Here, once more, it is revealed why the complex becomes destabilized on reduction: The two $(CuS)_3$ rings are pushed apart. The afore mentioned low lying MOs are weak Cu-N bonding MOs which did not occur in the other fragmentation due to their comparably low bonding contribution

Summing up, the bonding is mediated by a two to one mixture of covalent and donor–acceptor bonds between the Cu ions and the NGuaS ligand. The N-Cu bonding is of a coordinative character and weaker than the Cu—S bonds. The overall Cu. . .Cu interaction is antibonding but nevertheless the tight ring structure enables the formation of delocalized MOs over the whole Cu_6S_6 ring so the electrons can freely move within the torus. Those MOs show an equal distribution over all Cu ions albeit formally one finds four Cu(I) and two Cu(II) ions. The different oxidation states occur only as a perturbation to the overlying electronic structure manifesting in the last significant digits. This is in agreement with the EPR measurements and explains why there are no hyperfine splitting observed for the oxidized and reduced species.[45] The anisotropy of the g-tensor for the reduced state is <0.01 and nearly independent of the functional and basis. It fits compared to the experimental isotropic value 0.00.[45] For the oxidized state, the experiment finds an anisotropy of 0.08 where the calculations depending on functional and basis led to slightly larger values of 0.10 to 0.12. Looking at the spin densities, cf. Figure 7, one sees that for both species the signal is originating at the core and the expectation value of $<S^2> = 0.75$ shows that only a single electron distributed over the core is responsible for the signal. For the oxidized species, one sees that the spin density is not as equally distributed over the core as for the reduced one. This might be a first hint for the slightly deviation in the anisotropy between these states.

[†]The d-lobes in the *xy*-plane cannot be assigned to either the *x*- or *y*-axis but are rather aligned along the ring, hence the ϕ-direction in a cylindrical coordinate system.

Table 3. Wiberg bond orders (top) and total overlap population TOP in e– (bottom) for different calculated charged states, within TPSSh + D3BJ/def2-TVZp.

Complex charge	Cu-S (l)	Cu-S (s)	Cu-S (z)	Cu. . .Cu	Cu-N	S-C
$[Cu_6L_6]^{3+}$	0.59	0.52	0.33	0.15	0.48	0.90
	0.41	0.28	0.11	–0.09	0.29	0.89
$[Cu_6L_6]^{2+}$	0.56	0.53	0.32	0.16	0.40	0.92
	0.40	0.28	0.10	–0.14	0.24	0.89
$[Cu_6L_6]^{1+}$	0.52	0.52	0.31	0.15	0.34	0.93
	0.37	0.29	0.09	–0.17	0.17	0.84
$[Cu_6L_6]^{0}$	0.46	0.52	0.31	0.14	0.28	0.94
	0.32	0.31	0.08	–0.22	0.11	0.76

UV/Vis Spectroscopy

The experimental data as it is published in Ref. 45 is shown in Figure 8 along with the calculated TD-DFT spectra for the different oxidation states. From an experimental point of view, the spectra are interpreted in two sections: the intense low energy absorptions, greater than 1000 nm, are assigned to $\psi \rightarrow \psi^*$ transitions within the Cu_6S_6 core. In literature ψ and ψ^* are termed in the context of Cu_A as the bonding/antibonding frontier orbitals (especially H and L) distributed over the Cu core, cf. the work of Solomon.[6,72,73] For a realistic complex, the core bonding MOs are, as discussed above, considerably lower in energy, hence, we will drop these coined terms to avoid any confusion. The high energy peaks below 800 nm are assigned to thiolate-based ligand to metal charge transfer (LMCT) transitions.[45] The oxidized absorption looks quite the same as in the 2+ case, just slightly redshifted for the intense low energy peak, 1332 to 1117 nm. The reduced spectrum on the other side is more redshifted. However, without further analysis one cannot say if the

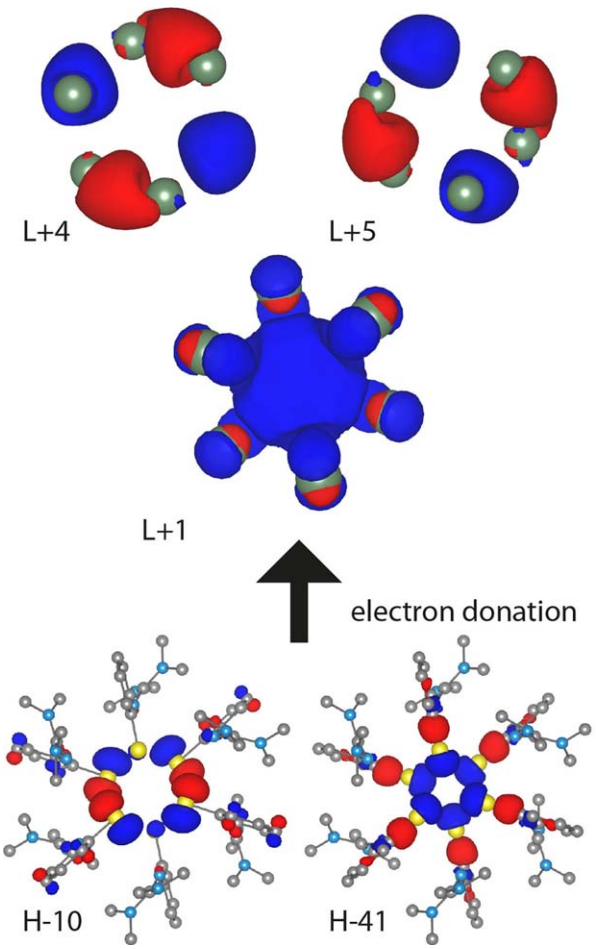

Figure 5. Most important FOs for the donor acceptor interaction at an isovalue of 0.035. [Color figure can be viewed at wileyonlinelibrary.com]

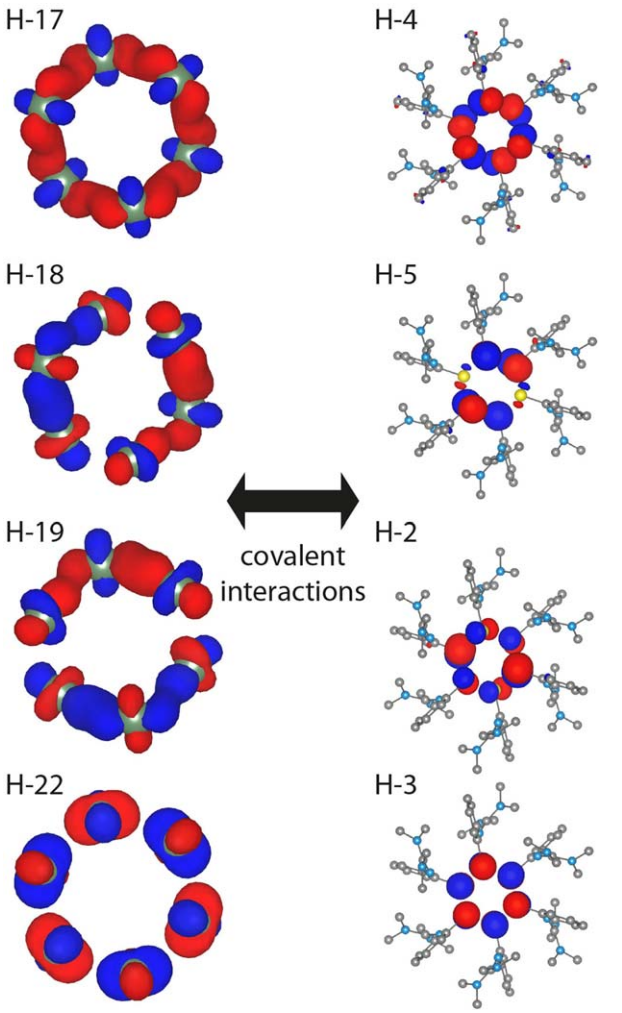

Figure 6. Main covalent contributing FOs, isovalue of 0.035. [Color figure can be viewed at wileyonlinelibrary.com]

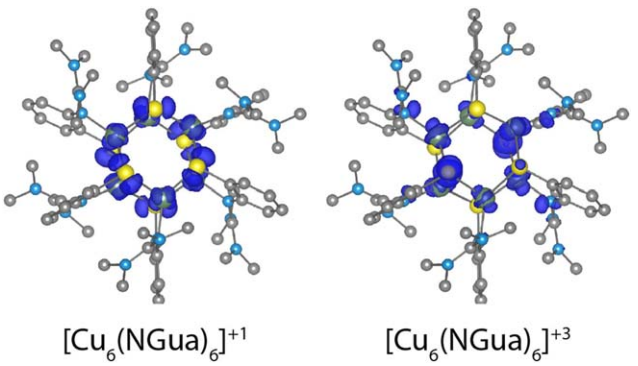

Figure 7. Spin densities of the $S = 1/2$ reduced and oxidized species. [Color figure can be viewed at wileyonlinelibrary.com]

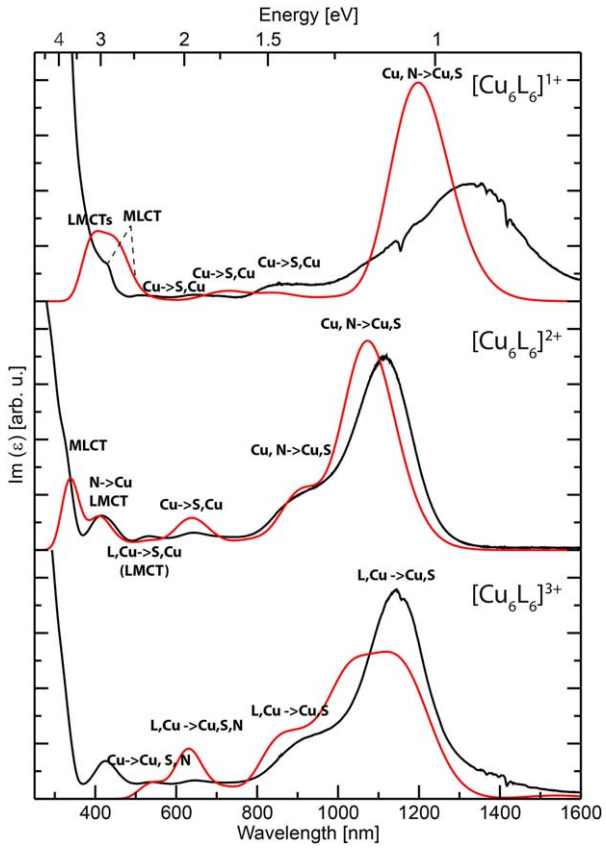

Figure 8. Experimental (black) as well as calculated (red) TD-DFT absorption spectra for the different charged states, with L = NGuaS. [Color figure can be viewed at wileyonlinelibrary.com]

peaks between 800 and 1000 nm are all the same peaks or different shifted peaks. By analyzing the calculated spectra, we will be able to distinguish and correlate the peaks.

As the experiment was performed in dichloromethane, the solvent is treated implicitly with a PCM. The possible impact of the solvent on the optical absorption spectra has already been discussed for the diamond core thiolate bridged copper complex. There the solvent gives rise to an energy level shifting as well as the removal of accidental degeneracy.[36] Hence, we do not want to discuss the influence of the solvent in detail, but rather immediately show the calculated spectra in the implicit solvent, Figure 8. The compiled experimental as well as the theoretical peaks are listed in Table 4. All absorptions greater than 355 nm are excitations into the LUMO, only for higher energies other unoccupied MOs are reached. The intense absorption band around 1000 nm with its shoulder is an absorption mainly within antibonding core MOs from Cu *d*, N *p* to the Cu *d*, S *p* LUMO. The same holds for the theoretical excitation around 640 nm, just that the N related orbitals are not excited anymore (compare Fig. 9a). The picture shifts toward the next calculated bands around 530 nm and 400 nm where one finds LMCT excitations from the N and C ligand atoms respectively with a small amount of Cu *d* to the Cu_6S_6 core, see Figure 9c. The last calculated excitation at 352 nm is a metal to ligand charge transfer (MLCT) where core electrons are excited toward the carbon atoms, see Figure 9d. This happens when the absorbed energy becomes high enough to excite into MOs higher than the LUMO. Thereby we find LMCT as well as MLCT transitions within one complex. A more complete list of the NTOs is given in S6.

The optical response of the oxidized state does not change much, as expected from the experimental observations. We find that calculated intensities as well as absorption frequencies do not change significantly between the theoretical $[Cu_6L_6]^{2+}$ and $[Cu_6L_6]^{3+}$ species. To keep the calculations feasible, we had to drop the polatization functions for the N atoms as well and still we could only calculate the spectrum up to an energy of 2.38 eV. The nature of the absorption bands changes only slightly. As the β HOMO LUMO gap is so small, both spin channels contribute already for low energy excitations leading to transitions which are mixed of LMCT and inner core Cu to Cu, S excitations, compare Table 4 and Figure 10. The splitting of the

Table 4. Measured and calculated absorption bands and the assigned major electronic excitation, wavelengths in nm.[a]

$[Cu_6L_6]^{3+}$			$[Cu_6L_6]^{2+}$			$[Cu_6L_6]^{1+}$		
Exp	Theo	Excitation	Exp.	Theo.	Excitation	Exp	Theo	Excitation
1145	1123	Ligand, Cu *d* → Cu *d*, S *p*	1117	1074	Cu *d*, N *p* → Cu *d*, S *p*	1332	1199	Cu *d*, N *p* → Cu *d*, S *p*
						1174	1197	Cu *d*, N *p* → Cu *d*, S *p*
						905	851	Cu *d* → Cu *d*, S *p*
950	954	Ligand, Cu *d* → Cu *d*, S *p*	960	914	Cu *d*, N *p* → Cu *d*, S *p*	860	743	Cu *d* → Cu *d*, S *p*
645	638	Ligand, Cu *d* → Cu *d*, S *p*, N *p*	640	629/667	Cu *d* → Cu *d*, S *p*	650	690	Cu *d* → Cu *d*, S *p*
537	535	Cu *d* → Cu *d*, S *p*, N *p*	530	536	Ligand, Cu *d* → Cu*d*, S *p*	545	523/572	Cu *d* → Cu *d*, S *p*
						515	462	Cu *d*, S *p* → Ligand
425		Not enough theoretical excitation states due to computational limits	420	408	Ligand, Cu *d* → Cu *d*, S *p*	430	432	Cu *d*, S *p* → Ligand
285			285	340	S *p*, Cu *d* → Ligand	259	398	Ligand → Cu *d*, S *p*

[a] Theoretical wavelengths are effective wavelengths, composed of several peaks, See S6 for a more detailed list. Lines are left empty to align associated excitations.

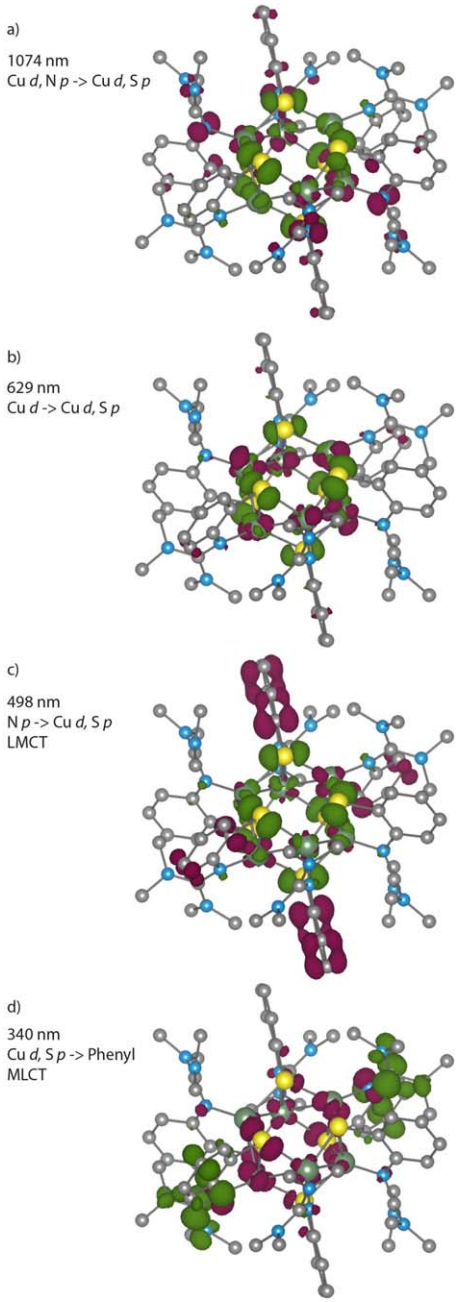

Figure 9. Visualization of characteristic transitions for $[Cu_6L_6]^{2+}$, see Figure 8, with the transition density, whereas purple displays charge depletion and green charge enhancement. [Color figure can be viewed at wileyonlinelibrary.com]

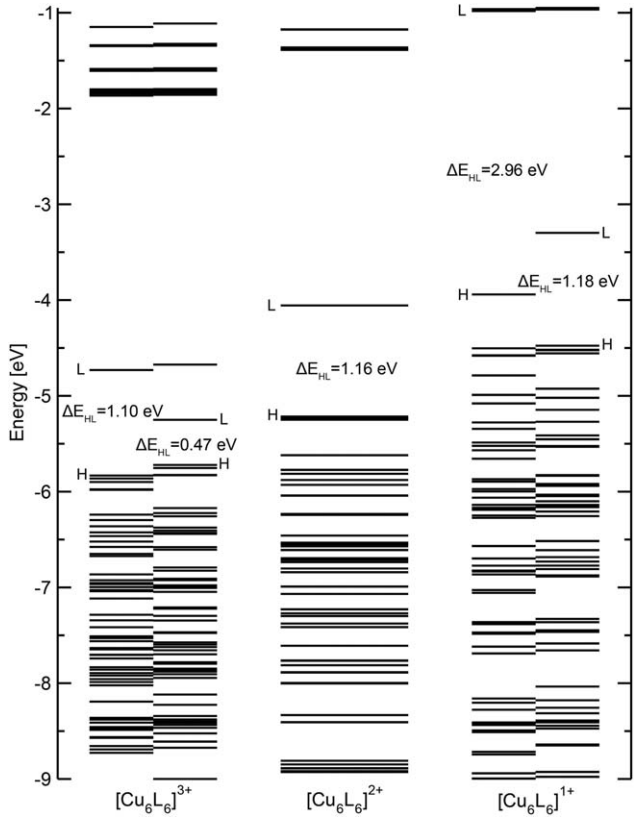

Figure 10. Calculated term scheme for the different charged states. Solvent DCM is included implicitly via PCM, whereas L = NGuaS.

first calculated low energy peak is due to two excitations where the LUMO and LUMO + 1 contribute differently, hence changing the excitation energy slightly, see Figure 10.

For the theoretical spectrum of the reduced species, one observes a larger redshift compared to the oxidized state as found in the experiment, $\Delta\lambda$=124 nm and $\Delta\lambda$=215 nm respectively. The energetic redshift between the two absorptions is 0.12 eV although the HOMO–LUMO gab widens up by 0.02 eV on reduction. Whereas the first excitation is composed of only one initial MO (H-3) for the reduced species, three MOs (H-3,H-4,H-7) donate charge in the 2+ species. Looking at the term scheme of the different charged states in Figure 10, it is notable that the H-7 is energetically significant below the other contributing MOs. This results in the observed redshift for the reduced species although the HOMO–LUMO gap even increases slightly. In the region between 1000 and 400 nm, a lowered experimental intensity can be observed. Down to around 470 nm all excitations are within one spin channel. The calculated intensities are diminished in agreement with the experiment. This was expected as only one half of the electrons can be excited resulting in a smaller effective cross section. Analyzing the peaks it is evident that experiment and calculated spectra correlate well. One finds that the experimentally expected LMCTs, which can be clearly identified for the $[Cu_6L_6]^{2+}$ state, are existent for the reduced species as well (below 398 nm) but blueshifted and mixed with absorptions within the core although, compare Table 4. Only for smaller wavelengths than 385 nm clear LMCTs are observable. Intuitively this is clear, as on reduction it becomes easier exciting electrons from the Cu atoms to the thiolates than reducing it further with LMCTs. From a theoretical point of view, one would argue with the oscillator strength f that enters Fermi's golden rule:

$$f = \frac{2|<i|\hat{p}|f>|^2}{m\hbar\omega}$$

As the bonding and antibonding Cu d, S p core orbitals are spatially strongly overlapping, the transition dipole matrix will be larger than for distant ligand orbitals.

The absorption spectra of the three different oxidation states are, compared to each other, quite similar despite their complex nature of absorption processes. Nevertheless is the intuitive interpretation, based on a class III Cu complex according to Robin and Day,[74] in principle correct although incomplete. Only a detailed orbital based analysis of each transition shows the existence of low wavelength transitions around 500 nm from bonding to antibonding core MOs and the fact that excitations within the Cu_6S_6 core dominate over a wide range (down to 500 nm) for the reduced and oxidized species. Comparing to the dinuclear NGuaS bridged complex, we can conclude that the characteristics for the high as well as the low wavelength spectrum are the same: Excitations within the core and MLCTs.

Conclusions

We analyzed the hexanuclear complex cation $[Cu_6L_6]$ composed of copper ions and bridging bifunctional thiolate-guanidine ligands. A detailed bonding analysis based on fragmentation and overlap population analysis shows that donor–acceptor bonding as well as classical two electron sharing covalent bonding mechanisms are both important for the stabilization of the complex. Delocalized FOs over the Cu_6 ring are important, being responsible for the whole Cu_6S_6 core forming a delocalized torus for the electrons. On reduction the torus expands and by integrating the charge, we show that more electrons are confined within the whole core structure. We can only speculate that this "electrostatic pressure" is the reason for the double reduced species not being obtainable in an electrochemical fashion.

The optical absorption spectrum is reproduced with the help of TD-DFT and implicit inclusion of the solvent effects. The shape as well as the absolute position of the absorption bands can be reproduced in very good agreement with the experiment irrespective of the nature of the excitation. We can assign the origin of the absorptions and find that excitations within the Cu_6S_6 core occur from long wavelengths down to 430 nm. LMCTs can be observed around 400 and 335 nm, whereas for higher energies MLCTs determine the absorption process. So, both charge transfer processes are present in this complex. The redshift of the $[Cu_6L_6]^{1+}$ spectrum is not related to a HOMO–LUMO gap closing but rather a simpler origin of the excitation: For the reduced $1+$ species, only MOs having higher eigenvalues are responsible for the excitation.

Keywords: density functional theory · time-dependent-DFT · copper thiolate complexes · charge decomposition analysis

How to cite this article: M. Witte, M. Rohrmüller, U. Gerstmann, G. Henkel, W. G. Schmidt, S. Herres-Pawlis. *J. Comput. Chem.* **2017**, *38*, 1752–1761. DOI: 10.1002/jcc.24798

Additional Supporting Information may be found in the online version of this article.

[1] P. Alemany, S. Alvarez, *Inorg. Chem.* **1992**, *31*, 4266.
[2] G. Aullón, G. Ujaque, A. Lledós, S. Alvarez, P. Alemany, *Inorg. Chem.* **1998**, *37*, 804.
[3] A. A. Palacios, G. Aullón, P. Alemany, S. Alvarez, *Inorg. Chem.* **2000**, *39*, 3166.
[4] C. Mealli, A. Ienco, A. Poduska, R. Hoffmann, *Angew. Chem. Int. Ed.* **2008**, *47*, 2864.
[5] E. I. Solomon, D. E. Heppner, E. M. Johnston, J. W. Ginsbach, J. Cirera, M. Qayyum, M. T. Kieber-Emmons, C. H. Kjaergaard, R. G. Hadt, L. Tian, *Chem. Rev.* **2014**, *114*, 3659.
[6] E. I. Solomon, X. Xie, A. Dey, *Chem. Soc. Rev.* **2008**, *37*, 623.
[7] E. I. Solomon, R. G. Hadt, *Coord. Chem. Rev.* **2011**, *255*, 774.
[8] K. W. Penfield, A. A. Gewirth, E. I. Solomon, *J. Am. Chem. Soc.* **1985**, *107*, 4519.
[9] S. E. Shadle, J. E. Pennerhahn, H. J. Schugar, B. Hedman, K. O. Hodgson, E. I. Solomon, *J. Am. Chem. Soc.* **1993**, *115*, 767.
[10] D. W. Randall, S. Debeer George, B. Hedman, K. O. Hodgson, K. Fujisawa, E. I. Solomon, *J. Am. Chem. Soc.* **2000**, *122*, 11620.
[11] E. I. Solomon, R. K. Szilagyi, S. DeBeer George, L. Basumallick, *Chem. Rev.* **2004**, *104*, 419.
[12] E. I. Solomon, B. Hedman, K. O. Hodgson, A. Dey, R. K. Szilagyi, *Coord. Chem. Rev.* **2005**, *249*, 97.
[13] E. I. Solomon, S. I. Gorelsky, A. Dey, *J. Comput. Chem.* **2006**, *27*, 1415.
[14] S. Iwata, C. Ostermeier, B. Ludwig, H. Michel, *Nature* **1995**, *376*, 660.
[15] M. Wilmanns, P. Lappalainen, M. Kelly, E. Sauer-Eriksson, M. Saraste, *Proc. Natl. Acad. Sci. USA* **1995**, *92*, 11955.
[16] T. Tsukihara, H. Aoyama, E. Yamashita, T. Tomizaki, H. Yamaguchi, K. Shinzawa-Itoh, R. Nakashima, R. Yaono, S. Yoshikawa, *Science* **1995**, *269*, 1069.
[17] G. Henkel, A. Müller, S. Weissgräber, G. Buse, T. Soulimane, G. C. M. Steffens, H.-F. Nolting, *Angew. Chem. Int. Ed.* **1995**, *34*, 1488.
[18] N. J. Blackburn, S. De Vries, M. E. Barr, R. P. Houser, W. B. Tolman, D. Sanders, J. A. Fee, *J. Am. Chem. Soc.* **1997**, *119*, 6135.
[19] E. C. Brown, N. W. Aboelella, A. M. Reynolds, G. Aullo, S. Alvarez, W. B. Tolman, *Inorg. Chem. Commun.* **2004**, *43*, 3335.
[20] K. Paraskevopoulos, S. V. Antonyuk, R. G. Sawers, R. R. Eady, S. S. Hasnain, *J. Mol. Biol.* **2006**, *362*, 55.
[21] S. Chakraborty, M. J. Polen, K. N. Chacón, T. D. Wilson, Y. Yu, J. Reed, M. J. Nilges, N. J. Blackburn, Y. Lu, *Biochemistry* **2015**, *54*, 6071.
[22] B. M. Hoffman, J. E. Roberts, M. Swanson, S. H. Speck, E. Margoliash, *Proc. Natl. Acad. Sci. USA* **1980**, *77*, 1452.
[23] T. H. Stevens, C. T. Martin, H. Wang, G. W. Brudvig, C. P. Scholes, S. I. Chan, *J. Biol. Chem.* **1982**, *257*, 12106.
[24] M. Gennari, J. Pécaut, S. DeBeer, F. Neese, M.-N. Collomb, C. Duboc, *Angew. Chem. Int. Ed.* **2011**, *50*, 5662.
[25] J. Chan, Z. Huang, M. Merrifield, *Coord. Chem. Rev.* **2002**, *234*, 319.
[26] G. Henkel, B. Krebs, *Chem. Rev.* **2004**, *104*, 801.
[27] B. Ruttkay-Nedecky, L. Nejdl, J. Gumulec, O. Zitka, M. Masarik, T. Eckschlager, M. Stiborova, V. Adam, R. Kizek, *Int. J. Mol. Sci.* **2013**, *14*, 6044.
[28] V. Calderone, B. Dolderer, H.-J. Hartmann, H. Echner, C. Luchinat, C. Del Bianco, S. Mangani, U. Weser, *Proc. Natl. Acad. Sci. USA* **2005**, *102*, 51.
[29] M. J. Stillman, *Coord. Chem. Rev.* **1995**, *144*, 461.
[30] M. Vasák, D. W. Hasler, *Curr. Opin. Chem. Biol.* **2000**, *4*, 177.
[31] M. Gennari, M. Lanfranchi, R. Cammi, M. A. Pellinghelli, L. Marchiò, *Inorg. Chem.* **2007**, *46*, 10143.
[32] E. Cariati, E. Lucenti, C. Botta, U. Giovanella, D. Marinotto, S. Righetto, *Coord. Chem. Rev.* **2016**, *306*, 566.
[33] J.-F. Song, S.-Z. Li, R.-S. Zhou, J. Shao, X.-M. Qiu, Y.-Y. Jia, J. Wang, X. Zhang, *Dalt. Trans.*, **2016**, *45*, 11883
[34] A. Neuba, R. Haase, W. Meyer-Klaucke, U. Flörke, G. Henkel, *Angew. Chem. Int. Ed.* **2012**, *51*, 1714.
[35] M. Witte, U. Gerstmann, A. Neuba, G. Henkel, W. G. Schmidt, *J. Comput. Chem.* **2016**, *37*, 1005.
[36] M. Witte, B. Grimm-Lebsanft, A. Goos, S. Binder, M. Rübhausen, M. Bernard, A. Neuba, S. Gorelsky, U. Gerstmann, G. Henkel, W. Gero Schmidt, S. Herres-Pawlis, *J. Comput. Chem.* **2016**, *37*, 2181.
[37] C. Trumm, O. Hübner, P. Walter, S. Leingang, U. Wild, E. Kaifer, B. Eberle, H.-J. Himmel, *Eur. J. Inorg. Chem.* **2014**, *2014*, 6039.
[38] S. Wiesner, A. Wagner, O. Hübner, E. Kaifer, H.-J. Himmel, *Chem. Eur. J.* **2015**, *21*, 16494.
[39] A. Ziesak, T. Wesp, O. Hübner, E. Kaifer, H. Wadepohl, H.-J. Himmel, *Dalt. Trans.* **2015**, *44*, 19111.
[40] M. Schatz, V. Raab, S. P. Foxon, G. Brehm, S. Schneider, M. Reiher, M. C. Holthausen, J. Sundermeyer, S. Schindler, *Angew. Chem. Int. Ed.* **2004**, *43*, 4360.

[41] D. Petrovic, L. M. R. Hill, P. G. Jones, W. B. Tolman, M. Tamm, *Dalt. Trans.* **2008**, *2008*, 887.
[42] O. Bienemann, A. Hoffmann, S. Herres-Pawlis, *Rev. Inorg. Chem.* **2011**, *31*, 83.
[43] A. Hoffmann, M. Rohrmüller, A. Jesser, I. Dos Santos Vieira, W. G. Schmidt, S. Herres-Pawlis, *J. Comput. Chem.* **2014**, *2014*, 2146.
[44] J. Stanek, T. Rösener, A. Metz, J. Mannsperger, A. Hoffmann, S. Herres-Pawlis, In Topics in Heterocyclic Chemistry; Springer International Publishing: Switzerland, **2015**; pp. 211–238.
[45] A. Neuba, U. Flörke, W. Meyer-Klaucke, M. Salomone-Stagni, E. Bill, E. Bothe, P. Höfer, G. Henkel, *Angew. Chem. Int. Ed.* **2011**, *50*, 4503.
[46] M. J. Frisch, G. W. Trucks, H. B. Schlegel, G. E. Scuseria, M. A. Robb, J. R. Cheeseman, G. Scalmani, V. Barone, B. Mennucci, G. A. Petersson, H. Nakatsuji, M. Caricatos, X. Li, H. P. Hratchian, A. F. Izmaylov, J. Blooine, G. Zheng, J. L. Sonnenberg, M. Hada, M. Ehara, K. Toyota, R. Fukuda, J. Hasegawa, M. Ishida, T. Nakajima, Y. Honda, O. Kitao, H. Nakai, T. Vreven, J. A. Montgomery, Jr., J. E. Peralta, F. Ogliaro, M. Bearpark, J. J. Heyd, E. Brothers, K. N. Kudin, V. N. Staroverov, R. Kobayashi, J. Normand, K. Raghavachari, A. Rendell, J. C. Burant, S. S. Iyengar, J. Tomasi, M. Cossi, N. Rega, J. M. Millam, M. Klene, J. E. Knox, J. B. Cross, V. Bakken, C. Adamo, J. Jaramillo, R. Gomperts, R. E. Stratmann, O. Yazyev, A. J. Austin, R. Cammi, C. Pomelli, J. W. Ochterski, R. L. Martin, K. Morokuma, V. G. Zakrzewski, G. A. Voth, P. Salvador, J. J. Dannenberg, S. Dapprich, A. D. Daniels, Ö. Farkas, J. B. Foresman, J. V. Ortiz, J. Cioslowski, D. J. Fox, Gaussian09, Revision D01; **2009**, Gaussian, Inc., Wallingford.
[47] J. Tao, J. Perdew, V. Staroverov, G. Scuseria, *Phys. Rev. Lett.* **2003**, *91*, 146401.
[48] V. N. Staroverov, G. E. Scuseria, J. Tao, J. P. Perdew, *J. Chem. Phys.* **2003**, *119*, 12129.
[49] V. N. Staroverov, G. E. Scuseria, J. Tao, J. P. Perdew, *J. Chem. Phys.* **2004**, *121*, 11507.
[50] M. G. Medvedev, I. S. Bushmarinov, J. Sun, J. P. Perdew, K. A. Lyssenko, Science **2017**, *355*, 49.
[51] S. Grimme, *J. Comput. Chem.* **2006**, *27*, 1787.
[52] S. Grimme, S. Ehrlich, L. Goerigk, *J. Comput. Chem.* **2011**, *32*, 1456.
[53] F. Weigend, R. Ahlrichs, *Phys. Chem. Chem. Phys.* **2005**, *7*, 3297.
[54] F. Weigend, *J. Comput. Chem.* **2006**, *8*, 1057.
[55] M. E. Casida, *J. Mol. Struct. THEOCHEM* **2009**, *914*, 3.
[56] M. E. Casida, In *Recent Advances in Density Functional Methods, Part 1;* World Scientific, Singapore, **1995**; p. 155.
[57] S. Miertus, E. Scrocco, J. Tomasi, *Chem. Phys.* **1981**, *55*, 117.
[58] M. Cossi, V. Barone, R. Cammi, J. Tomasi, *Chem. Phys. Lett.* **1996**, *255*, 327.
[59] M. Cossi, G. Scalmani, N. Rega, V. Barone, *J. Chem. Phys.* **2002**, *117*, 43.
[60] R. L. Martin, *J. Chem. Phys.* **2003**, *118*, 4775.
[61] A. J. Bridgeman, G. Cavigliasso, L. R. Ireland, J. Rothery, *J. Chem. Soc. Dalton Trans.* **2001**, 2095.
[62] (a) S. I. Gorelsky, **2013**. Available at: http://www.sg-Chem.net/ (b) S. I. Gorelsky, AOMix: Program for Molecular Orbital Analysis, http://www.sg-chem.net/, version 6.87, **2015**; (c) S. I. Gorelsky, S. Ghosh, E. I. Solomon, *J. Am. Chem. Soc.* **2006**, *128*, 278; (d) S. I. Gorelsky, A. B. P. Lever, *J. Organomet. Chem.* **2001**, *635*, 187.
[63] L. Noodleman, J. G. Norman, *J. Phys. Chem.* **1979**, *70*, 4903.
[64] L. Noodleman, *J. Chem. Phys.* **1981**, *74*, 5737.
[65] L. Noodleman, E. J. Baerends, *J. Am. Chem. Soc.* **1984**, *106*, 2316.
[66] L. Noodleman, D. Case, *Adv. Inorg. Chem.* **1992**, *38*, 423.
[67] R. Bauernschmitt, R. Ahlrichs, *J. Chem. Phys.* **1996**, *104*, 9047.
[68] H. B. Schlegel, J. J. W. McDouall, In Computational Advances in Organic Chemistry: Molecular Structure and Reactivity; C. Ögretir, I. G. Csizmadia, Eds.; Springer Netherlands: Dordrecht, **1991**; pp. 167–185.
[69] A. Neuba, U. Flörke, W. Meyer-Klaucke, M. Salomone-Stagni, E. Bill, E. Bothe, P. Höfer, G. Henkel, *Angew. Chem.* **2011**, *123*, 4596.
[70] J. Sun, A. Ruzsinszky, J. P. Perdew, *Phys. Rev. Lett.* **2015**, *115*, 036402.
[71] A. Oppermann, R. Dick, C. Wehrhahn, U. Flörke, S. Herres-Pawlis, G. Henkel, *Eur. J. Inorg. Chem.* **2016**, *2016*, 3744.
[72] D. R. Gamelin, D. W. Randall, M. T. Hay, R. P. Houser, T. C. Mulder, G. W. Canters, S. De Vries, W. B. Tolman, Y. Lu, E. I. Solomon, *J. Am. Chem. Soc.* **1998**, *120*, 5246.
[73] S. DeBeer George, M. Metz, R. K. Szilagyi, H. Wang, S. P. Cramer, Y. Lu, W. B. Tolman, B. Hedman, K. O. Hodgson, E. I. Solomon, *J. Am. Chem. Soc.* **2001**, *123*, 5757.
[74] M. B. Robin, P. Day, In *Advances in Inorganic Chemistry and Radiochemistry*, Academic Press, New York **1968**, Vol. 10, p. 247.

Received: 8 August 2016
Revised: 4 February 2017
Accepted: 11 March 2017
Published online on 10 April 2017